A Hybrid Artificial Neural Network and Wavelet Packet Transform Approach for Fault Location in Hybrid Transmission Lines

Narges Rezaee Ravesh[1], Nabiollah Ramezani[1], Iraj Ahmadi[1], Hassan Nouri[2]

[1]Department of Electrical & Computer Engineering, University of Science and Technology of Mazandaran, P.O.Box 48518-78195, Behshahr, Iran
[2] Power Systems and Energy Research Laboratory, the University of the West of England, (UWE) Bristol, UK
*ramezani@mazust.ac.ir

Abstract: This paper presents a single-ended traveling-wave-based fault location (F.L.) method in a hybrid transmission line (HTL) with an overhead section combined with a cable section. For this, the software has been developed in a MATLAB programming environment. Wavelet packet transform is used to extract transient information of the aerial mode current and voltage signals. The normalized current and voltage wavelet entropy (features) are fed to the feature selection part of the software. Regarding the HTL construction, the optimal features are obtained using the support vector machine and particle swarm optimization. A three-layer artificial neural network is trained to identify the faulty section and half using the optimal features of post fault signals. The square of the aerial mode voltage wavelet coefficients is applied to locate the fault using Bewley's diagram. The proposed approach is applied for F.L. in HTL. Transient simulations are obtained through EMTP-RV software for various fault scenarios, including fault types, resistances, inception angles, and locations. The post fault signals are fed to the developed software. The results illustrate the high accuracy of the proposed method in comparison to previous works.

Keywords: Hybrid transmission lines, Fault location, Feature selection, Bewley's diagram, Artificial Neural Network

List of Symbols and Abbreviations:

OHL: Overhead Transmission Lines
UGC: Underground Cable
W.T.: Wavelet Transform
DWT: Discrete Wavelet Transform
WPT: Wavelet Packet Transform
ANNBPR: Artificial Neural Network-based pattern recognition
FL: Fault Location
RBF: Radial Basis Function
SVM: Support Vector Machine
T.T.: Time-Time Transform
PSO: Particle Swarm Optimization
s_i: The i^{th} WPT coefficient of the signal s
x_i: Input data of the SVM classifier
Y_i: Labels of each Input data of the SVM classifier
α_i: Lagrangian coefficients of the Lagrange function for input data of the SVM classifier
M(α): Lagrange function
$k(x_i, x_j)$: Kernel function
C: parameter that relates to the penalty coefficient of the SVM classifier
b: Bias coefficient
sgn: Sign function.

γ: Standard deviation of the Gaussian function
$d(x)$: Decision-making function in SVM classifier
CF: Performance function
E_i: Error related to each KFold
K: Number of Folds
N: Total number of data
t: Target of the ANNBPR
y: Output of the ANNBPR
e: Cross entropy function for analyzing the performance of the ANNBPR
V^{cable} : Speed of the propagation of the wave in the cable section
V^{line} : Speed of the propagation of the wave in the overhead section
L_L : Length of the overhead section
L_C : Length of the cable section
L : Length of the overhead/cable section
$WTC^2_{DA_2}$: The Square of the coefficients of wavelet packet transform of the aerial mode voltage
E(s): Shannon Entropy of the signals

1. Introduction

1.1. Background and Motivation

Since overhead transmission lines (OHL) are exposed to damage due to natural disasters and have an undesirable impact on the landscape, hybrid transmission lines (HTL), which consist of overhead and cable sections, are used appropriately to the location [1-2]. Although underground cables (UGCs) benefit the environment and relieve public pressure, the expensive investment and high life cycle cost limit their use in the complete replacement of OHLs. Therefore, an HTL mainly consists of one or more OHL sections and one or more UGC sections, providing a trade-off between several issues such as investment, power transfer continuity, and environmental issues. In the case of a short circuit on transmission lines, the fault location (F.L.) must be determined swiftly and accurately to minimize transmission-line outage time, thereupon increasing system stability and decreasing system energy not supplied. F.L. methods are classified into three classes: impedance-based, traveling waves-based, and artificial intelligence-based [3].

The most common F.L. method is the impedance-based method, which calculates the fault distance by using the linear relationship between the F.L. and sequential impedance. In the case of underground cables (UGCs), the variation of the zero-sequence impedance regarding the different types of sheath grounding methods causes a non-linear relation between measured impedance and fault distance. As a result, the impedance-based method has encountered several problems for F.L. in UGCs and, consequently, in HTLs [2, 4]. More recently, traveling wave-based F.L. methods have attracted the attention of researchers owing to their high reliability and high speed in determining fault type and location. These methods need high sampling rate transformers. Due to advancements in power electronics and optical instrument transformers' production, high-frequency sampling for transient fault signal recording has been realized [5-7]. In single-ended traveling waves-based F.L. methods, the location of a short circuit can be calculated according to the time delay between the arrival times of the incident and reflected traveling waves of aerial mode voltage at the terminal.

Using the cross-correlation between the primary wave and the propagated wave is the basic and one of the most utilized methods for detecting the incident and reflected traveling waves on a transmission line [8]. This method needs

the exact selection of the time window length. At the same time, it depends on the F.L. The primary idea to solve this problem has been proposed in [9], which uses the discrete wavelet transform (DWT) for the information extraction of the transient wave. Different mother wavelets in various scales are utilized for arrival time detection, mainly dependent on test cases, noise severity, and sampling frequency [10-12]. In the case of an HTL, the main challenge in the traveling waves-based F.L. method is determining the fault section due to the inequality of the propagation speed on overhead and cable sections. A single-ended traveling wave-based F.L. method for HTL is presented in [13]. DWT, SVM, and Bewley diagrams are used to quickly extract information, faulty-section, and half identification and fault location. The accuracy of this method is not satisfactory in the case of high resistance faults or small fault inception angles due to generating small energies of voltage and current wavelet coefficients.

In [14], the F.L. is determined using the installed fault locators at both terminals of the HTL. In this method, the faulty section is determined by comparing the time delay and the arrival time of traveling waves to the two terminals concerning the default values. These fault locators are synchronized through 2 Megapixel optical fiber channels. Despite the high accuracy of this procedure, its increased investment cost has restricted its acceptability by power system operators. In [15], the wavelet coefficients of the aerial mode voltage have been used to find the faulty-section identification and F.L. The obtained results show the weak accuracy of this method. In addition, the used default value to find the F.L. depends on the network configuration.

The support vector machine (SVM) has been applied to determine the fault section on HTL [16]. In the proposed algorithm, the SVM inputs are the coefficients square of the aerial mode voltage in the DWT. This method has a low computational burden, but the method's accuracy when the fault occurs on half of the cable section is inappropriate.

In [17], a traveling-wave-based F.L. algorithm comprising a faulty-section identification and a F.L. method is presented for hybrid multi-terminal transmission systems. The main disadvantage of the proposed method is that it cannot find the fault section in some instances. In [18] for thyristor-controlled series- compensated lines, a novel protection method is presented based on the time-time (T.T.) transform. In the proposed algorithm, current signals at both sides of the sending and receiving ends are retrieved and processed through time-time domain transform (TT-transform), and a TT-matrix is produced. Although obtained results show suitable performance, the proposed method is not tested on HTL.

Most recently, a hybrid SVM-TT transform-based method for F.L. in HTL is presented [19]. Although the simulation results give satisfactory accuracy for a faulty section and half identification, this method suffers from high error in F.L., especially for the faults near the middle point of the overhead and cable sections. For example, in a reported case, the cable F.L. error is about 1.48% of total HTL length or 8.91% of the UGC length, equal to 2.85km.

In [20], a two aspects procedure based on wide-area traveling-wave has been proposed for F.L. in regional power grids. The proposed method is double-ended and is applied only to OHL. In [21], the F.L. technique is presented for three-terminal hybrid OHLs with one off-service line branch. The average obtained error is 1.65%, but the method is not tested on HTL.

1.2. Contributions

The delay between the arrival time of the initial traveling waves in the ground and aerial modes has been used previously for faulty-section and half identification on HTL. The accuracy of the results depends on fault type, fault inception angle, fault resistances, and fault location, while the F.L. error is high. Using a classifier leads to improved accuracy in the detection of the faulty section and half. In addition, the type of features used as inputs of the classifier for faulty-section and half identification have a high impact on distinguishing sections from each other. Available published F.L. methods use a trial and error approach to find the features which are not immune from the risk of the calculation errors.

F.L. methods based on DWT, T.T., and S transform show that the misclassification zone around the middle point of the overhead and cable sections is more than 1.48% of total HTL length (2.5 Km) for high-resistance faults or faults occurring at small inception angles. These errors for F.L., especially in the cable section, are so high.

In this paper, a single-ended method based on traveling waves has been proposed to compute the F.L. on HTL. This method uses WPT to extract the high-frequency data of the aerial mode current and voltage signals. Artificial Neural Network based pattern recognition (ANNBPR) classifiers are used for faulty-section and half identification. In the proposed algorithm to decrease the computational burden and the error of the ANNBPR classifiers, raised by trial and error, the optimal features of ANNBPR classifiers are calculated by a particle swarm optimization (PSO)-based feature selection procedure with SVM as the fitness function. Furthermore, the K-Fold validation method is used in the proposed feature selection method to avoid the dependence of SVMs on the training data. After identifying the faulty section and half by the neural network, Bewley's diagram of aerial mode voltage signal is used to determine the location of the fault. The WPT square coefficients of the aerial mode voltage are employed to extract the high-frequency data of the aerial mode voltage signal for F.L.

1.3. Paper Organization

The remainder of this paper is organized as follows. WPT and the mathematical formulation of the suggested model are presented in section 2. In section 3, the feature selection method based on PSO-SVM is presented. In section 4, the proposed F.L. method is introduced in detail. Section 5 includes the simulation results, and finally, section 6 concludes the paper.

2. Proposed structure of WPT decomposition

Wavelet Transform (W.T.) has several applications in the topic of signal processing in power systems, such as transient states analysis [22], power quality analysis [23], and harmonics analysis [24]. This transform uses the fast and slow changes of the waveform that correspond to the high frequency and low-frequency components of the signal, respectively. W.T. overcomes the limitations of the Fourier transform method, such as being a single-domain transform (i.e., only works in frequency domain) and its ability to eliminate sub and inter-harmonics.

In DWT, the input signal decomposes into approximated and detailed components using low and high pass filters. Afterward, only the approximated component is decomposed to extract the desired features of the signal. In WPT, the extended discrete form of the conventional W.T., both detailed and approximated components are decomposed simultaneously. As a result, WPT gives more information about the signal, has a better frequency resolution, and offers a more comprehensive view of the signal [25].

In this paper, the first cycle of the post fault of aerial mode current and voltage are decomposed to the third level, as shown in Fig. 1.

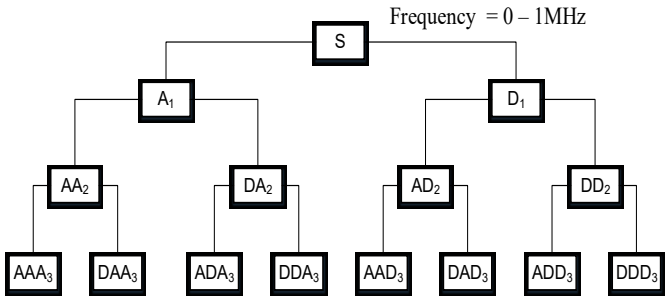

Fig. 1. *Structure of WPT decomposition*

Furthermore, the entropy criterion is the most common way to find the optimal decomposition in signal decomposition applications [26].

The statistical feature of the Shannon entropy is used for optimal decomposition. The feature matrix contains 30 features (one entropy statistical feature for fifteen coefficients of the WPT, each one for two signal types, 1×15×2=30). Entropy (E) is defined as an incremental cost function that E (0) =0. Shannon entropy is as follows [27]:

$$E(s) = -\sum_{i} s_i^2 \log(s_i^2) \qquad (1)$$

Some parameters can affect the amplitude of voltage and current signals and consequently the entropy values. This affection may lead to misclassification of features and subsequently introduce error in F.L. calculation. To make the proposed F.L. approach immune against this error, the normalized entropy values are used. The following formula is used for normalization.

$$y_i = \frac{(y_{max} - y_{min})}{(e_{max} - e_{min})} \times (e_i - e_{min}) + y_{min} \qquad (2)$$

Where e_i, e_{max} and e_{min} are the i^{th}, maximum and minimum values of the entropy vector of each feature, respectively. y_{max} and y_{min} are the upper and lower limits of normalization interval, respectively. In this paper y_{max} = +1 and y_{min} = -1.

3. Proposed feature selection method

Large-scale data raises the computational burden, despite creating opportunities in the study process. On the other hand, in most cases, all features of signals are not essential to make an appropriate classification. Furthermore, using all features decreases the efficiency of the learning algorithm [28, 29]. The feature selection method is an effective way to reduce the computational burden. Feature selection methods are categorized based on the generation and fitness functions.

The applied generation and fitness functions of the proposed method are introduced as follows:

3.1 Generation function

The generation function creates the candidate subsets among the features set. The number of possible subsets will be equal to 2^N features for a set of N data which is known here as the solution space. This number would be too high even for a small value of N. For this reason, using the optimization algorithms to search the solution space and find the near to optimum solution would be very efficient. According to [30, 31], the PSO has advantages over feature selection over other classical optimization algorithms. Therefore, in this research, the PSO algorithm is used as the generating function to select an optimal subset of the available features.

3.2 Fitness function

The fitness function of a single particle evaluates how close the particle is to the optimal point [32]. Hence, in this paper, errors of the SVM classifiers are used as a fitness function in feature selection. In the proposed method, three SVM classifiers are used to determine the optimal features for faulty-section and half identification. If a fault occurs on the overhead section, the output of SVM1 will be {+1}, but if it appears on the cable section, the outcome will be equal to {-1}. Furthermore, SVM2 and SVM3 are used to determine the faulty half of the overhead and cable sections, respectively. The output of SVM is {+1}, if the fault occurs on the first half of the overhead and cable section, and will be {-1} if the fault occurs on the second half of overhead or cable sections. The SVM classifier is briefly introduced as below.

Suppose that the data set is $\{(x_i, y_i)\}_{i=1}^{l} \in R^n \times \{-1, +1\}$ where x_i is the input data and y_i is the label of each x_i. The procedure is looking for a hyper plan in SVM that separates data with minimum error and maximum safety margin [33]. Whereas the used data in this paper is not linearly separable, this hyper plan can be achieved by solving the following optimization problem:

$$\begin{cases} \max M(\alpha) = -\frac{1}{2}\sum_{i=1}^{l}\sum_{i=1}^{l}\alpha_i\alpha_j y_i y_j k(x_i, x_j) + \sum_{i=1}^{l}\alpha_i \\ subject\ to: \ \sum_{i=1}^{l}\alpha_i y_i = 0\,, \quad 0 \le \alpha_i \le C\,, \quad i = 1,2,\dots,l \end{cases} \tag{3}$$

Where α_i is the Lagrangian coefficients of the Lagrange function, M(α), for each x_i, C is a parameter that relates to the penalty coefficient. The Kernel function $k(x_i, x_j)$ is used for mapping the data to a higher dimensional feature space where data is linearly separable in the new space. The decision-making function in the SVM is according to Eq. (4):

$$d(x) = sgn\left[\sum_{sv} y_i\alpha_i k(x_i, x_j) + b\right] \tag{4}$$

Among defined Kernel functions for SVM, the radial basis function (RBF) separates the data more accurately; therefore, this paper uses the radial basis function. This function is defined as follows [33]:

$$K(x_i + y_j) = exp\left(-\frac{\|x_i + y_j\|^2}{\gamma}\right) \tag{5}$$

In SVM, C determines the safety margin, and its lower values provide wider safety margins, and its higher values provide narrower safety margins. Furthermore, low values of γ cause that classifier to follow faster changes and the

Gaussian function to become sharp and have a better local function. Also, high values of γ cause the classifier to follow slower changes. Therefore, in this paper, two parameters of C and γ that will affect the accuracy and operation of SVM are determined using the PSO optimization algorithm.

In the proposed method to identify the faulty section and its corresponding half, optimal feature inputs of each ANNBPR are determined by the PSO-based feature selection method and the error of the SVM, as discussed earlier. In the proposed feature selection method, the error of SVM classifiers should have the minimum amount for the optimal feature subset which PSO obtains. Furthermore, to avoid the dependence of the SVMs model on the training data, the K-Fold validation method is used according to Fig. 2, which divides the data set into training and test sets. In other words, if F_i is a subset of entropy values of voltage and current, which are extracted from the WPT, then the performance function (C.F.) can be defined according to Eq. (6):

$$CF(F_i) = \frac{1}{k}\sum_{j=1}^{K} E_j(F_i) \qquad (6)$$

Where E_j is the error related to each KFold, K is the number of Folds. To achieve a reliable performance of the classifiers, the authors tested different values of K, and it is found that for k= 5, a more accurate classification output is obtained.

In Eq. (6), E_j for each one of three SVM functions is defined as follows:

$$E_j(F_i) = \frac{number\ of\ sample\ that\ have\ been\ incorrectly\ classified}{total\ number\ of\ sample\ tests} \qquad (7)$$

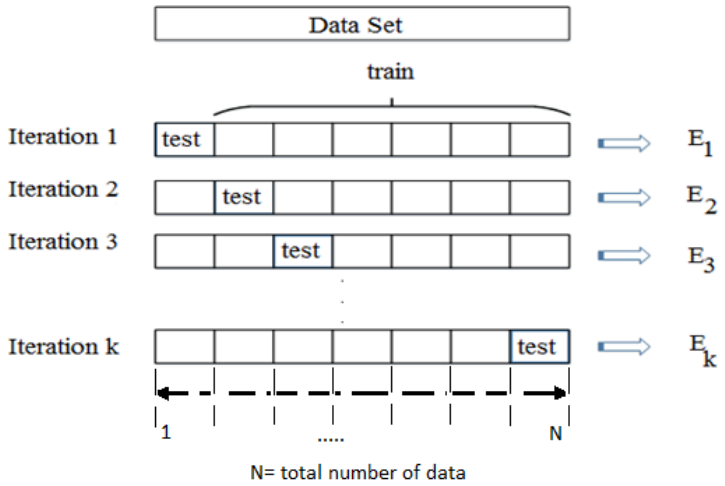

Fig. 2. *KFold cross-validation*

The arrangement of each particle in the process of optimal feature selection is shown in Fig. 3. Each particle is composed of three parts where the first two parts are related to SVM C and γ parameters, and the third part is made of a 1×30 dimension vector and contains random numbers between zero and one $(0 < f_i < 1)$ as random features. If the value of each $f_i (i \in \{1, 2, \ldots, 30\})$ is less than 0.5, then its corresponding feature will not be selected, and If the value of each f_i is more than 0.5, then its corresponding feature will be selected and applied to the decision function.

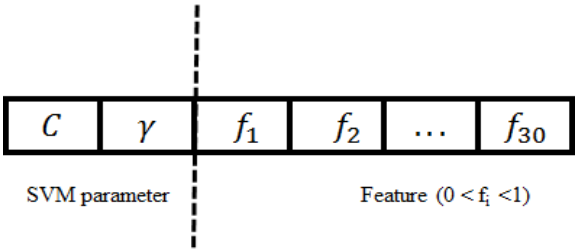

Fig. 3. *The structure of the SVM classifier particle*

The schematic diagram of the proposed feature selection method is shown in Fig. 4. The feature selection method is only performed one time for each ANNBPR. The method relies on the feature selection based on SVM-PSO to extract the best features, as opposed to the available published F.L. methods that use a trial and error approach to find the best features.

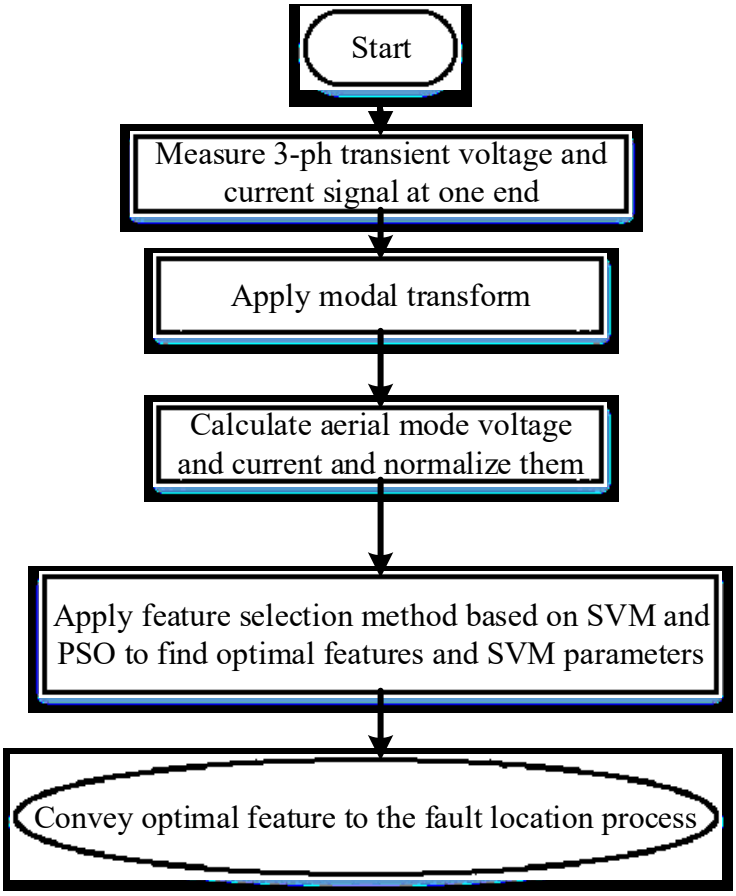

Fig. 4*. Schematic of the proposed feature selection*

4. Proposed FL algorithm

In this paper, the measured values of the aerial mode voltage at one terminal are used to determine the F.L. in HTL. The Schematic diagram of the proposed F.L. method is shown in Fig. 5.

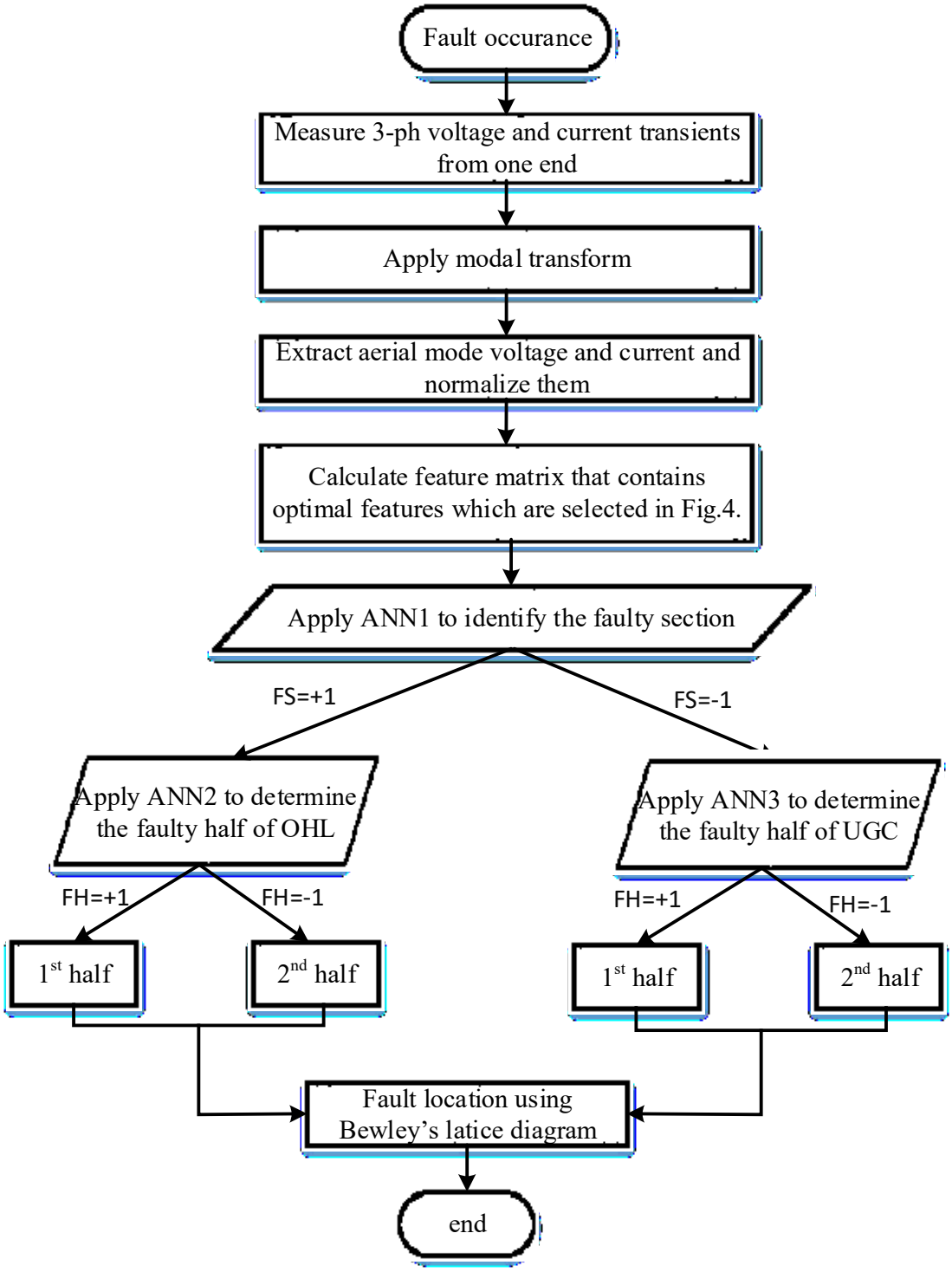

***Fig. 5**. Schematic diagram of the proposed fault location method*

The WPT is used to extract the information of the time-frequency domain of the aerial mode voltage signals obtained by EMTP_RV software. Optimal features as inputs of the classifier are determined by the feature selection method based on PSO-SVM. Therefore, the proposed algorithm consists of two steps as follows:

- Identification of faulty-section and its corresponding half by ANNBPR
- Determination of F.L. using Bewley's diagram.

These two steps are explained in sequence.

4.1 Identification of the faulty section and half

Using a time delay between ground and aerial mode voltages is the standard method to determine faulty-section of the OHL or UGC and its related half in previous works. In this paper, the ANNBPR classifiers are used for this purpose. ANNBPR is a powerful tool in pattern recognition and data classification. Pattern recognition networks are feed-forward networks that classify the inputs according to the specified target classes. Such ANNBPR often have one or more sigmoid hidden layers and one softmax output layer. The hidden layer has fifty neurons in this work, and the output layer has two neurons (two classes).

After fault occurrence, one cycle of the post fault three-phase voltages and currents at one bus is measured. The aerial mode voltage and current are computed using the Clarke transform and fed to the WPT. The outputs of WPT are the values of optimal features in the form of a matrix (i.e., feature matrix). The feature matrix is the input of all three ANNBPRs. If a fault occurs on the OHL, the output of ANNBPR1 will be {FS=+1}, but if it appears on the UGC, the output will be equal to {FS=-1}. Furthermore, ANNBPR2 and ANNBPR3 are used to determine the half faulty section of the OHL and UGC, respectively. When faults occur on the first half of OHL and UGC, outputs of ANNBPR2 and ANNBPR3 is +1 {FH=+1}, and for the second half of them equals -1{FH=-1}.

The structure of this network is shown in Fig. 6. The number of neurons is achieved by trial and error such that the error of the ANNBPR classifiers gets the least possible value. The Cross entropy function is used in these networks for analyzing the performance of the networks. The performance of the networks will be better with the lower output of the cross-entropy. This function can be defined for a two-class classifier as:

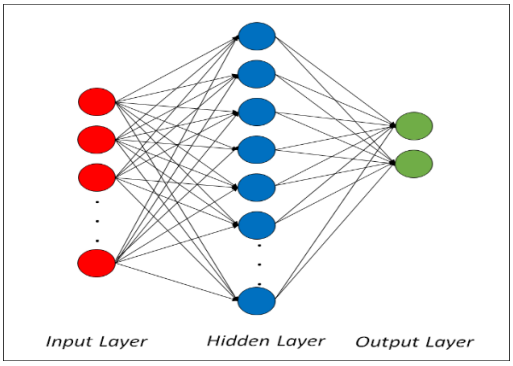

Fig. 6. *Structure of ANNBPR*

$$e = -t \times log(y) - (1 - t) \times log(1 - y) \quad (8)$$

The accuracy of each ANNBPR classifier can be calculated as:

$$Accuracy\ \% = (1 - e) * 100 \quad (9)$$

4.2 F.L. estimation

After identifying the faulty section and related half, it is possible to determine the exact location of the fault. At first, the square of DA_2 coefficients of the aerial mode voltage (i.e., WTC_{DA2}^2) are determined. Then the primary and secondary arrival times of the peak aerial mode voltage at the measuring device are calculated by WTC_{DA2}^2. Through calculated values, the behavior of the traveling wave has been investigated by Bewley's diagram. Finally, the location of the fault is calculated according to Table 1.

Table 1: The used Formula for calculating F.L. in various sections of HTL

Faulty-section	Faulty half (corresponding outputs of classifier)	Related formula
Overhead	First half (FS=+1 & FH=+1)	$\boldsymbol{x = \frac{V^{line} \times \Delta t}{2}}$
	Second half (FS=+1 & FH=-1)	$\boldsymbol{x = L_L - \frac{V^{line} \times \Delta t}{2}}$
Cable	First half (FS=-1 & FH=+1)	$\boldsymbol{x = L_L + \frac{V^{cable} \times \Delta t}{2}}$
	Second half (FS=-1 & FH=-1)	$\boldsymbol{x = L_L + L_C - \frac{V^{cable} \times \Delta t}{2}}$

5. The system under study and simulation results

The performance of the proposed F.L. method is evaluated on a 50 Hz, 230 kV HTL using EMPT-RV software. A single-line diagram of the HTL is depicted in Fig. 7. The lengths of the overhead section (L_L) and the cable section (L_C) are 100 miles and 20 miles, respectively. The measuring device is installed in location M at the beginning of the overhead section.

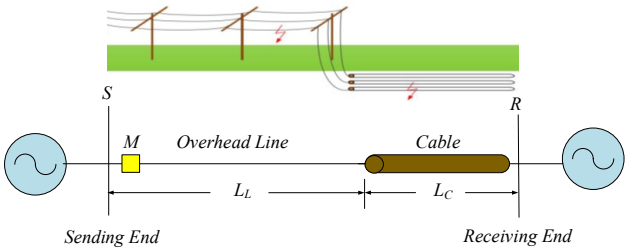

Fig. 7. *HTL under consideration*

The sampling frequency has been selected 1 MHz to increase the accuracy and resolution of the WPT. Also, db4 mother wavelet has been used to extract the transient information of the voltage and current signals. Moreover, the data of the overhead and the cable sections are taken from references [34] and [35], respectively, which have been shown in Appendix I. Frequency-dependent models are used to simulate the HTL sections. The aerial mode propagation speed of the traveling waves on the overhead and the cable sections have been calculated by EMTP-RV and are equal to 1.85×10^5 miles per second and 0.99×10^5 miles per second, respectively.

To evaluate the performance of the proposed method, we simulated 1350 different cases in the HTL, including different fault inception angles, fault locations, fault resistances, and fault types. The following values are used for this study:

1) Fault inception angles: 10^{o}, $125^{o,}$ and 260^{o} (i.e. 3 inception angles for all fault types, fault locations and fault resistances).
2) Fault resistance: 0.1Ω, 20Ω, and 100Ω (i.e. 3 resistances for 7 ground faults).
3) Fault locations: 10%, 20%, …, 80%, and 90% of the overhead and cable sections (i.e. 18 locations in combined line length).
4) Fault types: A.G., B.G., C.G., ABG, ACG, BCG, AB, A.C., BC, ABC, and ABCG (i.e. 11 types including 7 ground faults).

Therefore, 3×18× (3×7+4) = 1350 scenarios are simulated.

5.1. Optimum features for identification of the faulty section and half

To show the importance of selecting optimal features for the SVM classifier compared with selecting all features, the authors calculated the accuracy of the faulty-section and its corresponding half identification for all 1350 generated cases. The obtained results are presented in Table 2. PSO determines the optimal values of SVM parameters and optimum features (as input of ANNBPR classifier).

Table 2: Optimal selected features, parameters, and calculated accuracy of SVM classifiers

Type of classifier	With / Without feature selection	Calculated SVM parameters		Inputs for SVM		Accuracy of classifier (%)
		C	**γ**			
SVM1	Without feature selection	2.8480×10^{3}	1	Total features (30 features)		92
	With feature selection	7.5012×10^{3}	0.7883	Voltage	V_1, AA_2, DA_2, AAA_3, DAA_3, DDA_3, AAD_3, ADD_3, DDD_3	99.33
				Current	D_1, AD_2, AAA_3, DAD_3	
SVM2	Without feature selection	4.6210×10^{3}	0.9613	Total features (30 features)		92.15
	With feature selection	7.3824×10^{3}	0.8590	Voltage	V_1, AA_2, DA_2, DD_2, DAA_3, AAD_3, DAD_3, ADD_3, DDD_3	96.8
				Current	I_1, A_1, AA_2, AD_2, AAA_3, AAD_3, DAD_3	
SVM3	Without feature selection	7.1145×10^{3}	0.9944	Total features (30 features)		92.15
	With feature selection	6.2456×10^{3}	0.7433	Voltage	V_1, AA_2, AD_2, DD_2, AAA_3, DAA_3, ADA_3, AAD_3, ADD_3, DDD_3	96.9
				Current	A_1, AD_2, AA_3	

As explained in section 2, the feature matrix contains 30 features that 15 of which are related to aerial mode voltage, and the other 15 are about aerial mode current. Some of these features are selected by the feature selection method (using SVM+PSO) as optimal features. Based on this, 13 features (9 features of aerial mode voltage and 4 features of aerial mode current), 16 features (9 features of aerial mode voltage and 7 features of aerial mode current),

and 13 features (10 features of aerial mode voltage and 3 features of aerial mode current) are selected by SVM1, SVM2 and SVM3, respectively, as optimal features.

According to Table 2, using optimum features compared to all 30 features increases the accuracy of the faulty-section discrimination by 7.33%, faulty half in the overhead section by 4.65%, and faulty half in the cable section 4.75%.

It is worth noting that since the parameters C and γ have a significant influence on the accuracy of the SVM classifier, PSO also determines them for the case where all features are applied.

In the ANNBPR under study, 70 percent of the simulation results (i.e., 1350 different cases) are used as training data, 15 percent as test data, and the remaining 15 percent as validation data. To avoid dependency of ANNBPR output to training data, we performed data separation randomly and repeated it 200 times. The average of the errors calculated by Eq. (8) is considered the error of Pattern recognition.

Compression between the accuracy of the proposed approach (ANNBPR) and several other classifiers is presented in Table 3. Some other approaches, such as KNN [36] and SVM, are implemented in this paper. Also, the results of the proposed approaches in [13] and [19] are presented in Table 3 too. It should be mentioned that the same optimal features are considered for ANNBPR, SVM, and KNN to achieve a fair comparison.

Analysis of Table 3 shows that the accuracy of the proposed ANNBPR classifier in determining the faulty section and half is more than those obtained via SVM, KNN, and the proposed approach of [13]. Although the accuracy of [19] in detecting the faulty section is a bit better than the accuracy of this paper, investigation of the F.L. errors, presented in section 5.2., will illustrate the advantage of the method of this paper compared to [19].

Table 3: Comparison of different fault classifiers used in detecting the faulty section and half

Reference number	Feature selection	Fault classifier	Detection accuracy (%)		
			Faulty-section	Half section on overhead section	Half section on cable section
This paper	SVM+PSO	ANNBPR	99.58	98.61	97.08
		SVM	99.33	96.80	96.90
		KNN	96.96	90.37	81.33
[13]	Not used	SVM	98.8	98.2	95.60
[19]	Not used	SVM+PSO	99.8	98.9	97.50

5.2. Simulation result

In this section, the performance of the proposed approach is investigated by simulating faults in different sections and halves.

For the sake of clarification, a sample F.L. and error calculation are presented. For this purpose, phase A to ground fault (A.G.) has been simulated in the first half of the overhead section, 12 miles from the bus S. The fault resistance and inception angle are 100 ohms and 1°, respectively. The three-phase voltages before and after fault occurrence are depicted in Fig. 8.

Fig. 9 exhibits the $WTC^2_{DA_2}$ and the aerial mode voltage profiles. As shown in Fig. 9, the time difference between the primary and secondary peaks of the traveling wave is 127 microseconds.

If fault occurs on the overhead section, FS = +1, and FH=+1, using the equation of the first row of Table 1, F.L. can be calculated as follows:

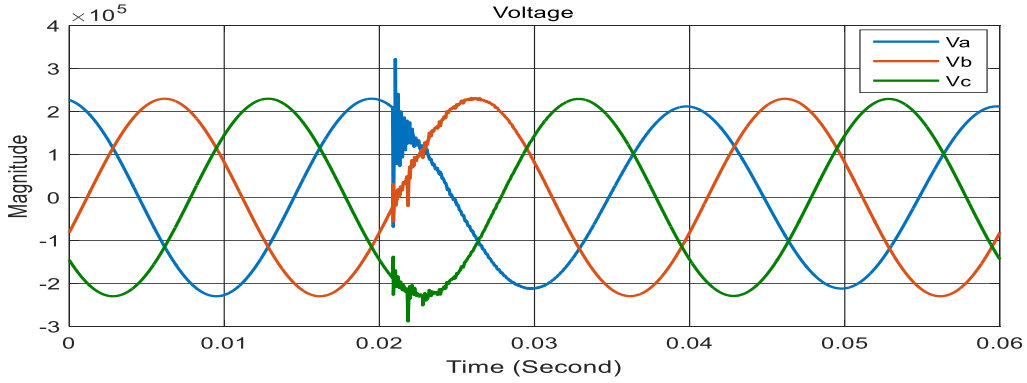

Fig. 8 *Pre-fault and post-fault three phase voltages for A.G. fault*

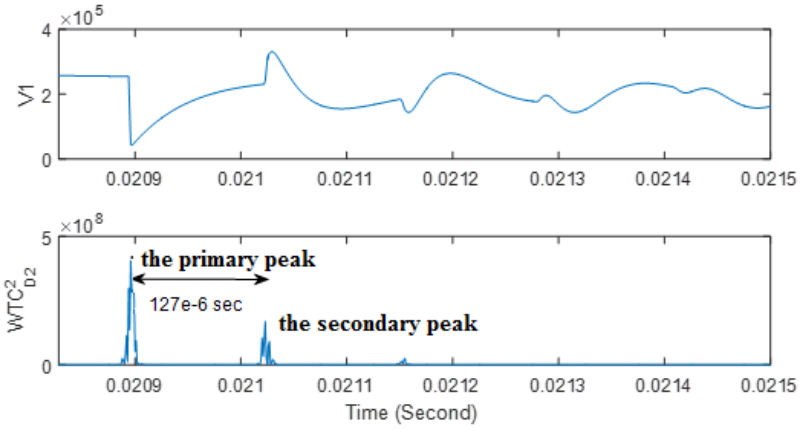

Fig. 9 *the aerial mode voltage and WTC² signals for A.G. fault scenario*

$$x = \frac{1.85 \times 10^5 \times 127 \times 10^{-6}}{2} = 11.89 mile$$

Based on the following equation, the F.L. error is - 0.11%.

$$\%E = \frac{d_{calculated} - d_{actual}}{L} \times 100 \qquad (10)$$

Where L is the length of the overhead/cable section.

A.G. faults with 0.5 Ω fault resistance in different distances have been studied. The results are presented in Table 4. The simulation results show that the calculation error is restricted to 0.41% and 1.2% in overhead and cable sections, respectively.

Table 4: Fault location error for different case

Fault section	Fault Distance from the beginning of the section (mile)	Outputs of classifier		Calculated fault location (miles)	Calculated absolute error (%)
		F.S.	F.H.		
Overhead section	5	1	1	4.81	0.19
	10	1	1	9.99	0.01
	20	1	1	19.98	0.02
	30	1	1	29.97	0.03
	40	1	1	39.59	0.41
	50	1	1	50.04	0.04
	60	1	-1	60.41	0.41
	70	1	-1	70.13	0.13
	80	1	-1	80.39	0.39
	90	1	-1	90.01	0.01
Cable section	2	-1	1	1.98	0.10
	4	-1	1	3.96	0.20
	6	-1	1	6.13	0.65
	8	-1	1	8.11	0.55
	10	-1	1	10.14	0.70
	12	-1	-1	11.89	0.55
	14	-1	-1	13.87	0.65
	16	-1	-1	16.24	1.2
	18	-1	-1	18.02	0.1

To compare the accuracy of the proposed method with recently published research [13, 19], we depicted the F.L. absolute error versus per unit fault distance for overhead and cable sections in Figs. 10 and 11, respectively.

According to Fig.10, the error of the proposed method in the entire overhead section is less than in previous works. Also, Fig.11 implies that the error of the proposed method is less than other works in the entire cable section.

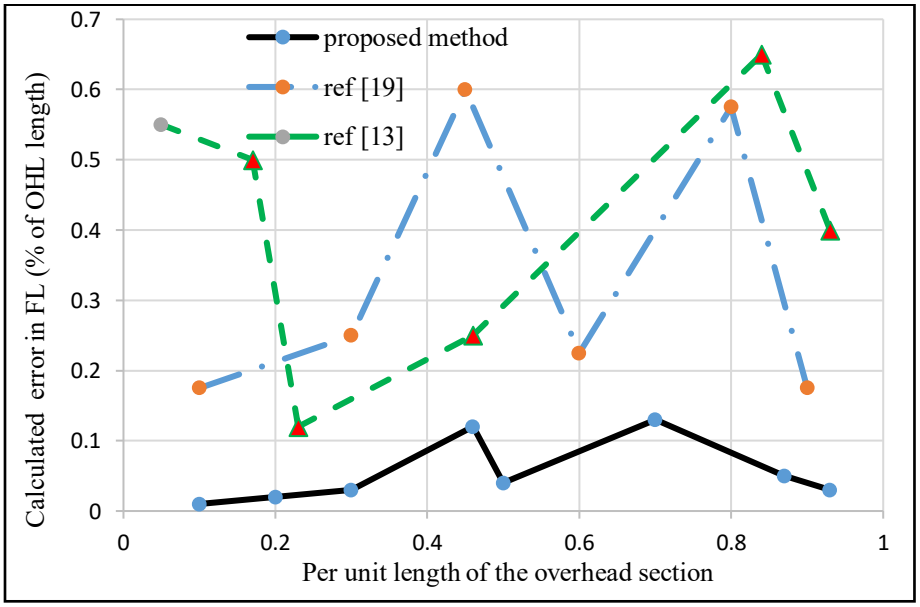

Fig. 10. *Overhead section F.L. error comparison between the proposed method and recently published research*

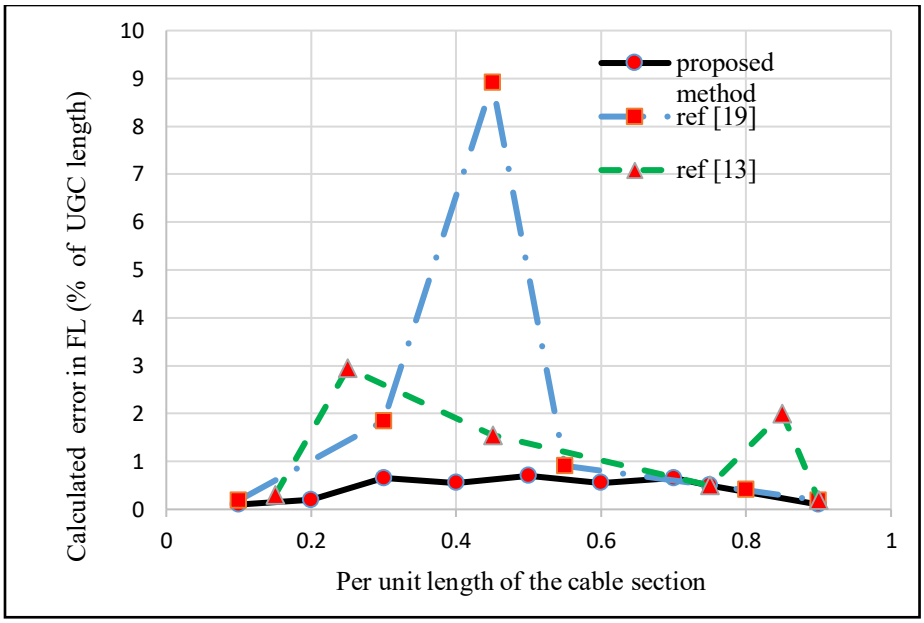

Fig. 11. *Cable section F.L. error comparison between the proposed method and recently published research*

The distribution of the obtained F.L. absolute errors in OHL and UGC sections is depicted in Fig. 12 in the form of box-plot form. Box-plot displays five statistical data: minimum, first quartile (Q1), median, third quartile (Q3), and maximum values of the corresponding data. The line that divides the box-plot into two parts is called median, in which half of the values are greater than or equal to this point, and the other half are less. 25 percent of the data fall below the Q1, and 25 percent are above the Q3.

Fig. 12 (a) shows that the F.L. absolute errors in the OHL section is distributed between 0.01% and 0.41%. The first quartile, the median, and the third quartile of the F.L. absolute errors in OHL section are 0.02%, 0.04%, and 0.39%, respectively. Furthermore, Fig 12 (b) illustrates the F.L. absolute errors in UGC spread out from 0.1% to 1.2% so that the first quartile, the median, and the third quartile are 0.20%, 0.55%, and 0.65%, respectively. The average absolute F.L. error is 0.161% and 0.522% in OHL and UGC sections, respectively.

5.3. Sensitivity analysis

The impact of some effective fault parameters such as fault type, resistance, and inception angle have been simulated, and the results are presented. It should be noted that the absolute F.L. errors are calculated based on Eq. (10).

5.3.1 The effect of fault resistance on F.L. accuracy

To evaluate the performance of the proposed method, the effect of various fault resistances ranging 0.01-100Ω in several arbitrary fault types and inception angles are studied as presented in Table 5. The results of this Table show that the error values are not affected by the value of fault resistance. It should be noted that, although the variation of the fault resistances strongly affects the intensity of the transient waves, since the normalized features are used as the input of ANNBPR, the F.L. accuracy is independent of the fault resistance value.

5.3.2 The effect of fault inception angle on F.L. accuracy

The impact of the fault inception angles ranging from 0 to 359 degrees is evaluated on the performance of the proposed method and the results are reported in Table 6. The study is carried out at a fixed fault type phase A to the ground (A.G.), random fault distances, and resistances. Analysis of the results indicates that the value of the inception angle does not significantly affect the F.L. accuracy.

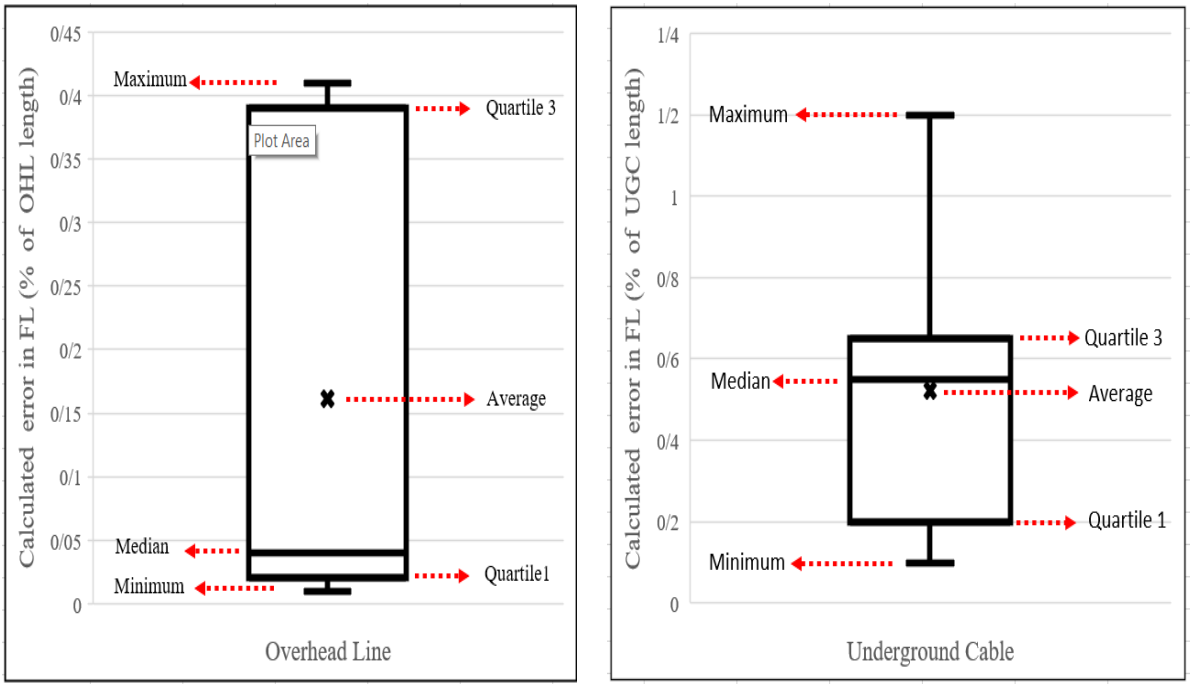

(a) (b)

Fig. 12. *Box plot of the absolute F.L. errors in (a) OHL section and (b) UGC section*

Table 5: Evaluating the impact of fault resistances on the performance of the proposed method

Fault type, location and inception angle	Fault resistance (Ohms)	Outputs of classifier		Calculated fault location (miles)	Calculated absolute error (%)
		F.S.	F.H.		
AG at 5 mile of HTL, δ=35°	0.01	1	1	4.81	0.19
	14	1	1		
	52	1	1		
	100	1	1		
ABG at 87 mile of HTL, δ=280°	0.01	1	-1	87.05	0.05
	14	1	-1		
	52	1	-1		
	100	1	-1		
CG at 105 mile of HTL (5 mile of cable section), δ=10°	0.01	-1	1	104.85	0.75
	14	-1	1		
	52	-1	1		
	100	-1	1		
ACG at 118 mile of HTL (18 mile of cable section), δ=40°	0.01	-1	-1	118.02	0.1
	14	-1	-1		
	52	-1	-1		
	100	-1	-1		

Table 6: Evaluating the impact of fault inception angle on the performance of the proposed method

Fault type, location and resistance	Fault inception angle (degrees)	Outputs of classifier		Calculated fault location (miles)	Calculated absolute error (%)
		F.S.	F.H.		
AG at 46 mile of line, RF=20 Ω	0	1	1	45.88	0.12
	10	1	1		
	35	1	1		
	80	1	1		
	300	1	1		
AG at 93 mile of line, RF=60 Ω	0	1	-1	92.97	0.03
	10	1	-1		
	35	1	-1		
	80	1	-1		
	300	1	-1		
AG at 102 mile of line (2 mile of cable), RF=0.1 Ω	0	-1	1	101.98	0.1
	10	-1	1		
	35	-1	1		
	80	-1	1		
	300	-1	1		
AG at 115 mile of line (15 mile of cable), RF=70 Ω	0	-1	-1	115.1	0.5
	10	-1	-1		
	35	-1	-1		
	80	-1	-1		
	300	-1	-1		

5.3.3. The effect of fault type on FL accuracy

The effect of the fault type on the performance of the proposed method under various fault distances, resistances, and inception angles has been evaluated and presented in Table 7. As seen, fault type, like other fault parameters, does not considerably impact the proposed F.L. performance.

Table7: Evaluating the impact of fault type on the performance of the proposed method

Fault distances, resistances and inception angle	Fault type	Outputs of classifier		Calculated fault location (miles)	Calculated absolute error (%)
		F.S.	F.H.		
at 46 mile of HTL (46 mile of overhead section), RF=20 Ω, δ=40°	AG	1	1	45.88	0.12
	BC	1	1		
	ACG	1	1		
	ABC	1	1		
at 99 mile of HTL (99 mile of overhead section), RF=50 Ω, δ=140°	BG	1	-1	98.98	0.02
	AC	1	-1		
	ABG	1	-1		
	ABC	1	-1		
at 105 mile of HTL (5 mile of cable section), RF=0.5 Ω, δ=80°	CG	-1	1	104.85	0.75
	BC	-1	1		
	ABG	-1	1		
	ABC	-1	1		
at 111 mile of HTL (11 mile of cable section), RF=25 Ω, δ=77°	AG	-1	-1	110.8	1
	AB	-1	-1		
	BCG	-1	-1		
	ABC	-1	-1		

6. Conclusions

In this paper, a single-ended method based on the feature selection approach and WPT is presented to locate the fault in a HTL. The transient information of the current and voltage signals is extracted from the corresponding sampled data during the first cycle of the post fault period. The information is then processed to obtain the entropy of the signals. The SVM algorithm and PSO algorithm are used to provide the optimal features and by this a better classification accuracy is achieved. A three-layer ANNBPR classified the faulty section and half. The required data for training of the ANNBPR are generated under different simulation scenarios. So, Bewley's diagram of the aerial mode voltage is used to locate the fault.

The proposed approach is applied to a 120-mile HTL (100-mile OHL + 20 mile UGC). The simulation results show the accuracy of distinguishing the faulty section is 99.58%, and the faulty half in overhead and cable sections is 98.61% and 97.08%, respectively. Also, the error of F.L. is restricted to 0.41% and 1.2% in overhead and cable sections, respectively.

The impact of various fault parameters such as type, resistance, and inception angle on the performance of the proposed method is evaluated. It is shown that the error of F.L. does not depend on these parameters.

The results of this paper are compared with two works in the area [13] and [19]. The accuracy of faulty-section, half detection, and F.L. of the proposed method is better than [13]. Although faulty-section and half detection accuracy is a little lower than of [19], the F.L. error in all cases, especially near the middle of the overhead and cable sections, is lower than [19].

7. References

[1] V. Leitloff, X. Bourgeat, G. Duboc, Setting constraints for distance protection on underground lines, 2001 Seventh Int. Conf. on Developments in Power System Protection (IEE), Amsterdam, Netherlands, April 2001.

[2] J. B. Lee, C.W. Ha, C.H. Jung, Development of digital distance relaying algorithm in combined transmission lines with underground power cables, 2001 Power Engineering Society Summer Meeting. Conference, Vancouver, BC, Canada, July 2001.

[3] P. Ray, D.P. Mishra, Support vector machine based fault classification and location of a long transmission line, Eng. Sci. Technol. Int. J., 19 (3), (2016), 1027-1039

[4] J. Han, P. Crosseley, Fault location on mixed overhead line and cable transmission networks, 2013 IEEE Grenoble Conf., Grenoble, France, Nov. 2013.

[5] M.M. Saha, J.J. Izykowski, and E. Rosolowski, Fault location on power networks' (London: Springer, 1st ed., 2010)

[6] IEEE PSRC Special Report, Practical aspects of Rogowski coil applications to relaying, IEEE Power Engineering Society, 2010.

[7] K.P.A.N. Pathirana, A.D. Rajapakse, O.M.K.K. Nanayakkara, and R. Wachal, Detecting fault generated surges in D.C. line of VSC HVDC schemes for travelling-wave based fault location, CIGRÉ Canada Conf., Montréal, Québec, Canada, 2012.

[8] M. Vitins, A correlation method for transmission line protection, IEEE Trans. Power App. and Sys. 97 (5), (1978), 1607-16178.

[9] F. H. Magnago, A. Abur, Fault location using wavelets, IEEE Trans. Power Del., 13 (4), (1998), 1475-1480.

[10] R. Jalilzadeh Hamidi and H. Livani, Traveling wave-based fault location algorithm for hybrid multi-terminal circuits, IEEE Trans. Power Del., 32 (1), (2017), 135-144.

[11] X. Lin, F. Zhao, G. Wu, Z. Li, and H. WengP, Universal wave front positioning correction method on traveling-wave-based fault location algorithms, IEEE Trans. Power Del., 27 (30), (2012), 1601-1610.

[12] S. M. Tayebi and A. Kazemi, A novel fault direction discrimination and location technique for three-terminal transmission lines, 2011 Int. Conf. on Applied Superconductivity and Electromagnetic Devices, Sydney, Australia, Dec. 2011, 92-96.

[13] H. Livani, C. Y. Evrenosoglu, A machine learning and wavelet-based fault location method for hybrid transmission lines, IEEE Trans. Smart Grid, 5 (1), (2014), 51-59.

[14] P.Chen, K.Wang, Fault location technology for high-voltage overhead lines combined with underground power cables based on travelling wave principle, 2011 IEEE Int. Conf. on Advanced Power System Automation and Protection (APAP) , Beijing, China, Oct. 2011.

[15] H.Livani, C. Y. Evrenosoglu, A traveling wave based single-ended fault location algorithm using DWT for overhead lines combined with underground cables, 2010 IEEE Power and Energy Society General Meeting, Providence, RI, USA, Jul. 2010.

[16] H.Livani, C. Y. Evrenosoglu, A hybrid fault location method for overhead lines combined with underground cables using DWT and SVM, 2012 IEEE Power and Energy Society General Meeting, San Diego, CA, USA, Jul. 2012.

[17] R.J. Hamidi, H. Livani, Traveling-wave-based fault-location algorithm for hybrid multi-terminal circuits', IEEE Trans. Power Del., 32 (1), (2017), 135–144.

[18] O.A. Gashteroodkhani, B. Vahidi, A. Zaboli, Time-time matrix z-score vector-based fault analysis method for series-compensated transmission lines, Turk. J. Electr. Eng. Comput. Sci., 25, (2017), 2647–2659.

[19] O.A. Gashteroodkhani, M. Majidi, M. Etezadi-Amoli, A.F. Nematollahi, B. Vahidi, A hybrid SVM-TT transform-based method for fault location in hybrid transmission lines with underground cables, Electr. Power Syst. Res., 170, (2019), 205–214.

[20] Z. X. Li ,Y. X. Cheng ,X. Wang ,Z. H. Li ,H. Weng, Study on wide-area traveling wave fault line selection and fault location algorithm, Int. Trans. Electr. Energy Syst., 28 (12), (2018), e2632.

[21] Y.Y. Lee, Ch-H. Chao, Tzu-Ch Lin, Ch-Wen Liu, A synchrophasor-based fault location method for three-terminal hybrid transmission line with One Off-service line branch'. IEEE Trans. on Power Del., 33 (6), (2018), 3249 – 325.

[22] D. C. Robertson, O. I. Camps, J. S.Mayer and W. B. Gish, Wavelet and electromagnetic power system transients, IEEE Trans. Power Del., 11 (2), (1996), 1050-1057.

[23] S. Santoso, E. J. Powers, W. M. Grady, and P. Hofman, Power quality assessment via wavelet transform analysis, IEEE Trans. Power Del., 11 (2), (1996), 924-930.

[24] Zh. Tongxin., E. B. Makram, and A. A. Girgis, Power system transient and harmonic studies using wavelet transform, IEEE Trans. Power Del., 14 (4), (1999), 1461 – 1468.

[25] B.K. Panigrahi, V.R. Pandi, Optimal feature selection for classification of power quality disturbances using wavelet packet-based fuzzy k-nearest neighbour algorithm, IET Gener. Transm. Distrib. , 3 (3), (2009), 296 – 306.

[26] Wavelet Packets - MATLAB & Simulink - MathWorks, www.mathworks.in/help/wavelet/ug/wavelet-packets.html.

[27] R. R. Coifman, M. V. Wickerhauser, Entropy-based algorithms for best basis selection, IEEE Trans. Informat. Theory, 38 (2), (1992), 713–718.

[28] P. Luukka, Feature selection using fuzzy entropy measures with similarity classifier, Expert Sys. Appl., 38 (4), (2011), 4600–4607.

[29] O. Maron, A. Moore, The racing algorithm: model selection for lazy learners, Artif. Intell. Rev., 11 (1), (1997), 193–225.

[30] S. Ding, L. Chen, Intelligent Optimization Methods for High-Dimensional Data Classification for Support Vector Machines, Intell. Informat. Manag., 2 (6), (2010), 159-168.

[31] S. W. Lin, K. C. Ying, S. C. Chen, Z. J. Lee, Particle swarm optimization for parameter determination and feature selection of support vector machines, Expert Sys. Appl., 35 (4), (2008), 1817–1824.

[32] O. Villacampa, Feature selection and classification methods for decision making: A comparative analysis, Doctoral dissertation, Nova Southeastern University, Retrieved from NSU Works, College of Engineering and Computing, 2015.

[33] J. Kamruzzaman, R. K. Begg, Support vector machines and other pattern recognition approaches to the diagnosis of cerebral palsy gait, IEEE Trans. Biomed Eng., 53 (12), (2006), 2479-2490.

[34] C.Y. Evrenosoglu, A. Abur, Travelling wave based fault location for teed circuits, IEEE Trans. Power Del., 20 (2), (2005), 1115-1121.

[35] T.C. Yu and J. R. Marti, A robust phase-coordinates frequency-dependent underground cable model (Zcable) for the EMTP, IEEE Trans. Power Del., 18 (1), (2003), 189-194.

[36] M. Cover and P. E. Hart, Nearest neighbor pattern classification, IEEE Trans. Informat. Theory, 13 (1), (1967), 21-27.

Appendix I

- Parameters of the system under study

Receiving and sending end voltage source parameters [13]	
Positive sequence impedance (Z1)	1.96 + j 4.70 Ω
Zero sequence impedance (Z0)	1.44 + j 4.39 Ω
Frequency of the system	50 Hz

- Configuration of overhead transmission line and cable [10]

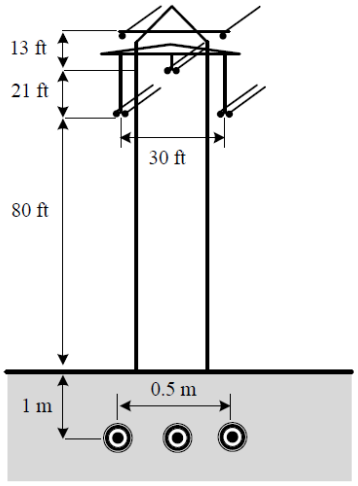

phase	Inside radius of core [cm]	Outside radius of core [cm]	Inside radius of sheath [cm]	Outside radius of sheath [cm]	Outer insulation Radius [cm]	Resistivity of core [Ω/m]	Resistivity of sheath [Ω/m]
A	0	2.34	3.85	4.13	4.84	0.017e-6	0.21e-6
B	0	2.34	3.85	4.13	4.84	0.017e-6	0.21e-6
C	0	2.34	3.85	4.13	4.84	0.017e-6	0.21e-6

- EMTP_RV data for 230kv overhead transmission line [10]

- EMTP_RV data for cable [10]

Phase	skin	DC Resistance [Ω/mile]	Outside Diameter [inches]	Horizontal Distance [ft]	Vertical Height at tower [ft]	Number of bundles
ground	0.5	6.74	0.36	45	114	0
ground	0.5	6.74	0.36	75	114	0
A	0.5	0.0984	1.196	60	101	2
B	0.5	0.0984	1.196	45	80	2
C	0.5	0.0984	1.196	75	80	2